JOURNAL OF GEOPHYSICAL RESEARCH, VOL. 100, NO. A10, PAGES 19,177–19,190, OCTOBER 1, 1995

Observations of plasmas and magnetic fields in Earth's distant magnetotail: Comparison with a global MHD model

L. A. Frank,[1] M. Ashour-Abdalla,[2,6] J. Berchem,[2] J. Raeder,[2]
W. R. Paterson,[1] S. Kokubun,[3] T. Yamamoto,[4] R. P. Lepping,[5]
F. V. Coroniti,[6] D. H. Fairfield,[5] and K. L. Ackerson[1]

Abstract. We are reporting the first direct comparison of in situ observations of plasmas and magnetic fields in Earth's distant magnetotail with the results of a time-dependent, global magnetohydrodynamic (MHD) simulation of the interaction of the solar wind with the magnetosphere. The magnetotail observations were taken with the Geotail spacecraft during the period 0300–0630 UT on October 27, 1992 at a position near the dawnside magnetopause at a downstream distance of about 81 R_E. During this period a dense, cold ion stream similar in density and speed to that expected for the magnetosheath plasmas was intermittently observed. When the cold ion stream was not present, the spacecraft was located in the northern magnetotail lobe. The dense, cold ion stream differed from that expected for the magnetosheath in the Y and Z components of ion bulk flow and in the Y component of the magnetic field. These cold ion streams are associated with a magnetopause accommodation region positioned just outside the classical magnetopause, as identified by a well-defined transition from magnetic fields typical of those found in the lobe to the lesser and more fluctuating fields in the magnetosheath. This accommodation region exhibits perturbations in plasma flows and magnetic fields that appear to be related to the complex topology of the magnetopause at these large downstream positions. Simultaneous observations of the solar wind ions and the interplanetary magnetic field (IMF) with the IMP 8 spacecraft upstream from Earth provided the driving input for a global MHD model. The solar wind ion flow was steady during this period, and the IMF exhibited a series of rotations from northward to duskward. The dynamics of the magnetotail were controlled by the Y and Z components of the IMF. When this B_Y was strongly positive, the magnetotail lobe appeared at the downstream Geotail position. Examination of the modeled plasma parameters in the Y–Z plane through the spacecraft position shows that this B_Y provides a torque on the magnetotail about its central axis. The MHD model also accurately positions the spacecraft alternately in the magnetopause accommodation region and the magnetotail lobe as the IMF clock angle varied from northward to duskward, respectively. The temporal variations of modeled parameters, i.e., ion densities, temperatures, and bulk flow velocities and the magnetic field components, are directly compared with the Geotail measurements. This first comparison of the Geotail observations with the modeled plasma parameters and magnetic fields provides substantial encouragement that a global MHD model can provide a valid description of important aspects of the large-scale topology and dynamics of the magnetotail.

[1]Department of Physics and Astronomy, The University of Iowa, Iowa City.
[2]Institute of Geophysics and Planetary Physics, University of California at Los Angeles.
[3]Solar-Terrestrial Environment Laboratory, Nagoya University, Toyokawa, Aichi, Japan.
[4]Institute of Space and Astronautical Science, Sagamihara, Kanagawa, Japan.
[5]NASA/Goddard Space Flight Center, Greenbelt, Maryland.
[6]Department of Physics and Astronomy, University of California at Los Angeles.

Paper number 95JA00571.
0148-0227/95/95JA-00571 $05.00

1. Introduction

In recent years a number of global magnetohydrodynamic (MHD) simulation models of the interaction of the solar wind with the magnetosphere have been developed [*LeBoeuf et al.*, 1978, 1981; *Lyon et al.*, 1981; *Wu et al.*, 1981; *Brecht et al.*, 1982; *Ogino*, 1986; *Fedder and Lyon*, 1987; *Watanabe and Sato*, 1990]. In general, these models used an idealized solar wind input to study the principal features of its coupling with the magnetosphere. Specifically, many studies employed a steady southward interplanetary magnetic field (IMF) to investigate the physics of substorms [*LeBoeuf et al.*, 1978, 1981; *Lyon et al.*, 1981; *Brecht et al.*, 1982;

Ogino, 1986; *Watanabe and Sato,* 1990; *Walker et al.,* 1993; *Raeder,* 1994]. *Usadi et al.* [1993] reported the results of a recent simulation of the magnetotail for both southward and northward IMF. *Ogino et al.* [1992, 1994] and *Raeder et al.* [1995] used global MHD simulations to study the dynamics of the magnetosphere for northward IMF. The ionospheric current–voltage relationship was also investigated by *Fedder and Lyon* [1987]. *Fedder and Lyon* [1987] and *Fedder et al.* [1991] have provided simulation results for the energy coupling between the solar wind and the magnetosphere as a function of the IMF clock angle.

Recently, simultaneous observations of plasmas and magnetic fields that are suitable for testing the MHD simulation models for Earth's magnetotail have become available. Although measurements of the magnetic fields in the distant magnetotail have been previously published [*Slavin et al.,* 1985], the plasma observations were incomplete; for example, there were no observations of the thermal ions [*Bame et al.,* 1983]. These ion observations were subsequently acquired during the Galileo fast flyby through the magnetotail [*Frank et al.,* 1993, 1994a] and the extensive survey now being conducted with the Geotail spacecraft [*Frank et al.,* 1994b, c; *Frank and Paterson,* 1994; *Paterson and Frank,* 1994]. Fortunately, the solar wind plasmas and the IMF were simultaneously monitored with IMP 8 during a substantial portion of these magnetotail observations.

Our present work is directed toward a comparison of the results from a MHD–Ionosphere model of the magnetospheric interaction with the solar wind [*Raeder et al.,* 1995; *Berchem et al.,* 1995] with Geotail observations along the dawnside flank of the magnetotail at about 81 R_E downstream from Earth. These observations were taken during a period with relatively steady solar wind conditions and northward IMF. The dynamical responses of the magnetotail as seen at the Geotail position are primarily due to temporal variations in the Y and Z components of the IMF. When the Y component is weak or negative and the field is directed generally northward, a dense, cold ion stream is seen at the spacecraft position. During those periods for which the Y component is strongly positive the spacecraft is found to be in the northern magnetotail lobe. This initial comparison with a single series of observations and simulated results is expected to be followed by further examples for different solar wind and IMF conditions and positions within the magnetotail in order for us to fully investigate the effectiveness of the model. This initial comparison of observation and simulation results provides considerable encouragement that modeling of the complex global topology and dynamical responses of the magnetotail can be effective in the interpretation of measurements from a single spacecraft.

This paper begins with a presentation of a marvelous set of simultaneous observations of plasmas and magnetic fields in the solar wind with IMP 8 and in the magnetotail with Geotail. This is followed by an overview of the MHD–Ionosphere model. The observed solar wind parameters with the time–varying IMF are used as the driving input to this model in order to compute the plasma parameters and magnetic fields at the Geotail position. These computational results are then compared with the observations.

2. Observations

A series of simultaneous observations of the solar wind ions and the IMF with IMP 8 and of plasmas and magnetic fields in the magnetotail with the Geotail spacecraft is used to investigate the effectiveness of the global MHD–Ionosphere model. The Massachusetts Institute of Technology (MIT) plasma instrument [*Bellomo and Mavretic,* 1978] and the Goddard Space Flight Center (GSFC) magnetometer [*Lepping et al.,* 1992] were used to provide the interplanetary parameters. The plasma instrumentation and magnetometers on board the Geotail spacecraft are described by *Frank et al.* [1994b] and *Kokubun et al.* [1994], respectively. The period of primary interest is 0300–0630 UT on October 27, 1992. At 0530 UT the position of IMP 8 was $\mathbf{X}$ = (−0.9, −27.8, 16.0 R_E) in Earth–centered solar–ecliptic (GSE) coordinates, and the downstream location of Geotail was $\mathbf{X}$ = (−81.6, −10.6, 4.2 R_E) in Earth–centered solar–magnetospheric (GSM) coordinates. IMP 8 observed the solar wind at the above location because its dynamic pressure was unusually high.

An overview of the plasma observations with the comprehensive plasma instrumentation (CPI) on board Geotail is given by the energy–time (E–t) spectrograms of the hot plasma (HP) analyzer's responses to electrons and positive ions as shown in Plate 1. This analyzer provides measurements of the three–dimensional velocity distributions of positive ions and electrons over the energy–per–unit charge range 1 V ≤ E/Q ≤ 48 kV. On the right–hand side of the plate is shown the Geotail position (red dot) and a portion of the trajectory with tic marks for 1–day intervals. Nominal positions for the bow shock and the magnetopause are also shown. The bow shock is located in accordance with the results of *Slavin and Holzer* [1981], and the magnetopause is based upon the models reported by *Fairfield* [1971] and *Petrinec et al.* [1991]. This magnetopause position is consistent with the measurements with Explorers 33 and 35 [*Howe and Binsack,* 1972]. The upper four E–t spectrograms on the left–hand side of Plate 1 correspond to the responses of the HP analyzer to positive ions with velocity vectors within the solid angles indicated by the diagram on the right–hand side of each spectrogram. For example, the solid angle for the top spectrogram is centered on velocity vectors directed tailward. The responses of the HP analyzer to ions are summed over three complete instrument cycles and are color coded according to the color bar at the top of Plate 1. The responses are plotted as functions of E/Q and universal time in hours. The corresponding time resolution is 72.5 s, and the units below the color bar are counts. Note that the ion intensities in the fourth spectrogram are generally larger than those in the third spectrogram. This asymmetry in the responses indicates that the ion bulk flow is directed signifi-

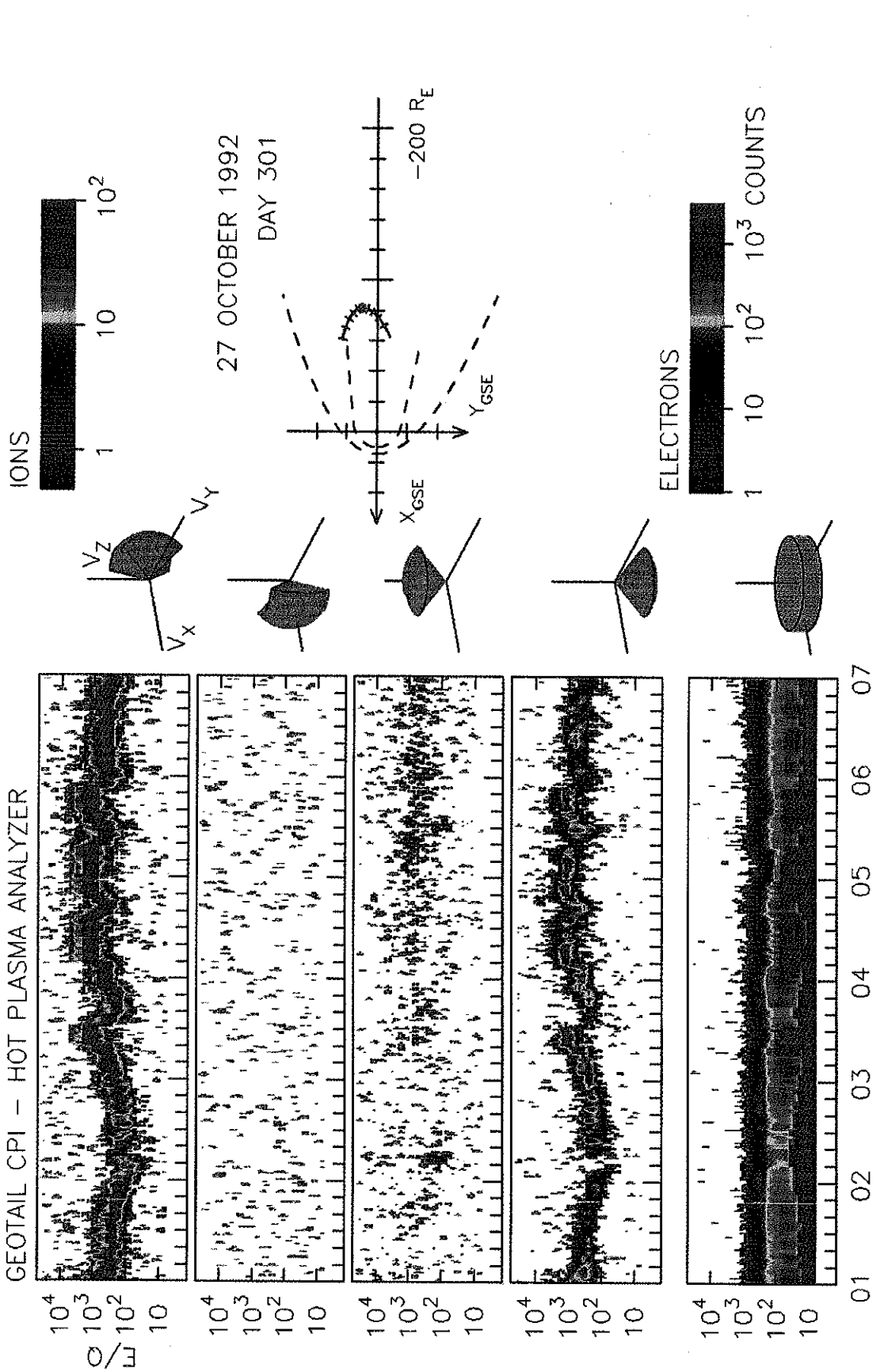

Plate 1. Energy–time (E–t) spectrograms of the responses of the hot plasma (HP) analyzer of the comprehensive plasma analyzer (CPI) on board the Geotail spacecraft during 0100–0700 UT on October 27, 1992. The format is explained in detail in the text. The upper four spectrograms are for positive ions, and the bottom spectrogram is for the electrons. The top spectrogram shows the presence of ions streaming in the antisunward direction and with varying density and speed. The diagram on the right-hand side of the plate indicates that the spacecraft is in the dawnside of the magnetotail.

cantly southward of the ecliptic plane. The *E–t* spectrogram at the bottom of Plate 1 shows the responses of the HP analyzer to electrons. As indicated by the diagram at the right-hand side of this spectrogram, the responses are summed for the plane that is perpendicular to the spacecraft spin axis, i.e., velocity vectors parallel to the ecliptic plane. The color bar for the electron responses is shown in the lower right-hand corner of Plate 1.

The purpose of the present work is to interpret the fluctuations of the plasma densities and flow speeds that are evident in the upper spectrogram of Plate 1 in terms of the responses of the magnetotail to variations in the IMF. In order to extend this interpretation to evaluations of the global magnetotail dynamics the computational results from the MHD–Ionospheric model are compared with the observations. Our first step is to compare the simultaneous measurements of plasmas and magnetic fields from Geotail and IMP 8.

Observations of the densities, temperatures, and components of the bulk velocities of ions with Geotail and IMP 8 are shown in Figure 1 for the period 0300–0630 UT. IMP 8 measurements in the upstream interplanetary medium are given by the thinner lines and are available for only part of this period. These interplanetary data have been plotted with a time delay of 20 min in order to account for the transit time for the solar wind from the position of IMP 8 to that of Geotail. As shown in the third panel of Figure 1, the solar wind speed is about 500 km/s. The Geotail plasma parameters are derived from the responses of the solar wind (SW) analyzer of the CPI. The ion densities in the magnetotail exhibit considerable fluctuations as a dense, cold ion stream is sporadically detected. This cold ion stream is detected four times during the series of measurements shown in Figure 1. The ion density and temperature and the *X* component of bulk flow velocity are similar to those observed in the solar wind with IMP 8. For those intervals during which the ion stream is not present the densities are lesser by factors of 10 or more, and the tailward bulk flow speeds decrease to values in the range of 100–300 km/s. Of greatest interest is the interval 0520–0610 UT for which there is a continuous series of observations from both spacecraft. During this interval a complete cycle for the presence and absence of a cold ion stream is recorded at the Geotail spacecraft. The two vertical dashed lines at 0526 UT and 0545 UT correspond to the absence and presence of the cold ion stream, respectively. Magnetotail cross sections for these times as derived from the MHD–Ionosphere model will be presented in the next section. Examination of the plasma parameters in Figure 1 shows that the characteristics of the cold ion stream are quite similar to those of the solar wind ions. Thus an interpretation of the cold ion stream as simply magnetosheath plasma is plausible. However, there are two features of the bulk flow velocity that suggest that an interaction with the magnetopause is occurring. That is, the deflection of the plasma in the $-Z$ direction is about 50 km/s, and the large, positive *Y* component of this bulk flow is about 70 km/s. In the dawnside magnetosheath this latter component is

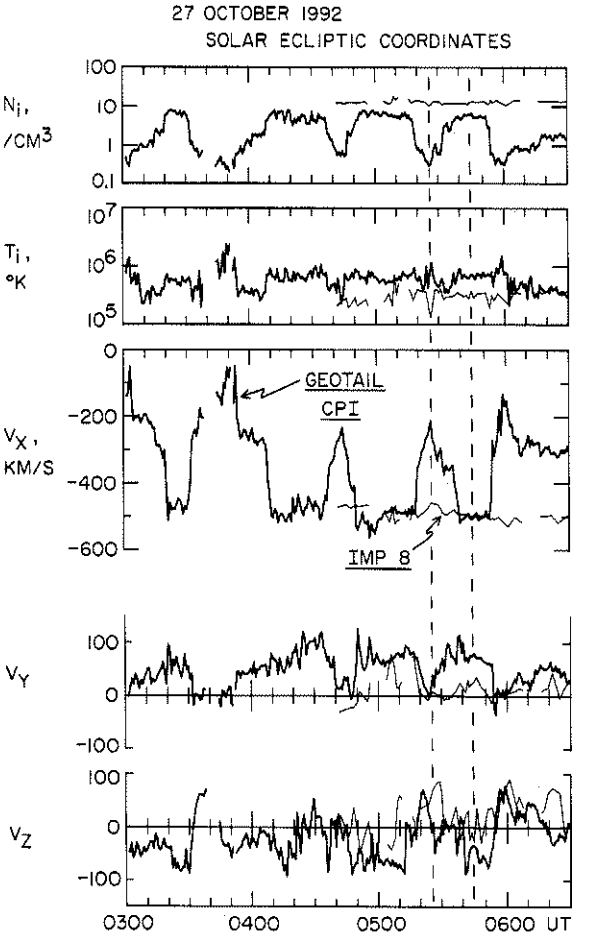

Figure 1. Observations of plasmas with the comprehensive plasma instrumentation (CPI) on board the Geotail spacecraft (thick lines) and with the IMP 8 MIT plasma analyzer (thin lines) during 0300–0630 UT on October 27, 1992. IMP 8 is positioned in the upstream solar wind and Geotail is located in the distant magnetotail near the dawnside magnetopause. A propagation delay of 20 min is added to the IMP 8 time line to account for the time required for the solar wind to pass from the location of IMP 8 to that of Geotail. The two vertical dashed lines at 0526 UT and 0545 UT occur for intervals for which a dense, cold ion stream is absent and present, respectively, at the Geotail spacecraft.

expected to be less than that of the solar wind, in this case, negative.

Further evidence that the cold ion stream is influenced by the immediate presence of the magnetopause is provided by the observations of magnetic fields with Geotail and IMP 8 that are shown in Figure 2. Inspection of the second and third panels of this figure shows that the interplanetary field generally exhibits a series of rotations from northward to duskward, i.e., from $+Z$ to $+Y$. In the top panel the *X* component of the magnetic field at the Geotail position clearly identifies the intervals for the appearances of the cold ion stream and the excursions into the northern magnetotail lobe. The lobe is identified with magnitudes of 12 to 15 nT and relatively low levels of fluctuations. Note that the *X* component of

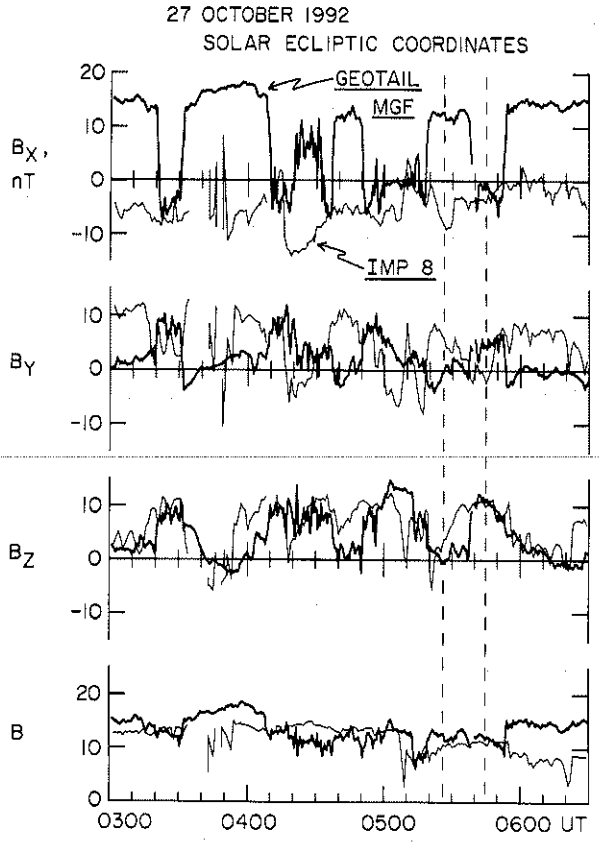

Figure 2. Continuation of Figure 1 for measurements of the magnetic fields with the Geotail magnetometer (MGF) and of the interplanetary magnetic field (IMF) with the GSFC magnetometer on board IMP 8. Note that the IMF undergoes a series of rotations from northward (+Z) to duskward (+Y) and that the northern magnetotail lobe appears at the Geotail position in response to a positive Y component of the IMF, e.g., at 0526 UT.

the magnetic field within the cold ion stream is not greatly dissimilar to that observed in the interplanetary medium. The controlling factor in the dynamical behavior of the magnetotail for this series of observations appears to be the Y and Z components of the IMF. When a strong duskward component is present, the magnetotail lobe appears at the Geotail position. When this component is small or directed dawnward and the IMF rotates northward, then the ion stream is present at Geotail. In the ion stream the Y component of the magnetic field is generally larger and positive, providing further evidence that the ion stream is a magnetosheathlike plasma that is affected by the nearby presence of the magnetopause. Of course, these plasmas are of directly magnetosheath origins.

3. The Global MHD–Ionosphere Model

A newly developed global single–fluid MHD code is used for this study. This code includes an ionospheric model for the closure of field–aligned currents. In order to accommodate the large simulation volume and long simulation times, both with good resolution, the simulation code was parallelized for multiple instruction–multiple data (MIMD) computers by using a domain decomposition technique. Only a brief description is given here; a more detailed presentation is given by *Raeder* [1994] and *Berchem et al.* [1995]. The model is derived from the ideal MHD equations for the magnetosphere and a potential equation for the ionosphere. However, because of the numerical methods, diffusion and resistive effects occur in the MHD solutions. These effects permit viscous interactions and, to some extent, magnetic field reconnection. In some cases the numerical resistivity is too low to allow for sufficient reconnection rates along the magnetopause and within the magnetotail current sheet. For this reason a resistive term has been included in Ohm's law and is described below.

The magnetospheric part of the model is solved for by a finite difference method which is conservative for the gasdynamic part of the MHD equations.

$$\frac{\partial \rho}{\partial t} = -\nabla \cdot (\rho \mathbf{v})$$

$$\frac{\partial \rho \mathbf{v}}{\partial t} = -\nabla \cdot \left(\rho \mathbf{v}\mathbf{v} + p\underline{\underline{I}}\right) + \mathbf{j} \times \mathbf{B}$$

$$\frac{\partial e}{\partial t} = -\nabla \cdot \{(e + p)\mathbf{v}\} + \mathbf{j} \cdot \mathbf{E}$$

$$\frac{\partial \mathbf{B}}{\partial t} = -\nabla \times \mathbf{E}$$

$$\nabla \cdot \mathbf{B} = 0$$

$$\mathbf{E} = -\mathbf{v} \times \mathbf{B} + \eta \mathbf{j}$$

$$\mathbf{j} = \nabla \times \mathbf{B}$$

$$e = \frac{1}{2}\rho v^2 + \frac{p}{\gamma - 1}$$

where ρ is the plasma mass density, $\mathbf{v}$ is the flow velocity, p is the plasma pressure, $\underline{\underline{I}}$ is the unit tensor, $\mathbf{E}$ and $\mathbf{B}$ are the electric and magnetic fields, respectively, $\mathbf{j}$ is the current density, and the ratio of specific heats is $\gamma = 5/3$. The resistive term that has been included in Ohm's law is a nonlinear function of the local magnetic field gradients. This resistivity is

$$\eta = \alpha j_1^2$$

with

$$j_1 = \begin{cases} j_2 & \text{if } j_2 \geq \delta \\ 0 & \text{otherwise} \end{cases}$$

and

$$j_2 = \frac{|\mathbf{j}|\Delta}{|\mathbf{B}| + \varepsilon}$$

where $\mathbf{j}$ is the local current density, $\mathbf{B}$ is the local magnetic field, Δ is the grid spacing, and ε is a very small number to avoid division by zero. The normal-

ized current j_2 ($0 \le j_2 \le 1$) is used as a switch for the resistivity. Where the resistivity is switched on it becomes proportional to the square of the local current. Similar resistivity models have been used in the past to model the kinetic effects that lead to anomalous resistivity [*Sato and Hayashi,* 1979; *Ugai,* 1985]. The parameters α and δ determine the value of the resistivity and the current threshold that must be reached for the resistivity to be switched on, respectively. The resistivity η is only nonzero at a few grid points in strong current sheets.

The numerical grid is rectangular and nonuniform with the highest spatial resolution near Earth (about 0.5 R_E). It extends 30 R_E in the sunward direction, 250 R_E in the tailward direction, and ±70 R_E in the Y and Z directions, respectively. The gasdynamic part of the equations is spatially differenced by using a technique in which fourth-order fluxes are hybridized with first-order [*Russanov,* 1962] fluxes [*Harten and Zwas,* 1972; *Hirsch,* 1990]. The magnetic induction equation is treated differently to ensure that $\nabla \cdot \mathbf{B} = 0$ by following a method outlined by *Evans and Hawley* [1988] for exactly satisfying this relationship. The time stepping scheme for all variables consists of a low-order predictor with a time-centered corrector, which is second-order accurate in time. The outer boundary conditions are fixed by the given solar wind values on the upstream side of the bow shock. At the other boundaries, open boundary conditions are applied, i.e., zero normal derivative.

The inner boundary where the MHD model is connected to the ionosphere is taken to be a spherical shell with radius 3.7 R_E and centered on Earth. The choice of this radius is a compromise that is guided by numerical necessities such as extremely high Alfvén speeds and very large magnetic field gradients close to Earth. However, the proper mapping of all relevant field-aligned current systems is accommodated. Inside the spherical shell the MHD equations are not solved and a static dipole field is assumed. The important physical processes within the shell are the flow of field-aligned currents (FACs) and the closure of these currents in the ionosphere. At each time step the magnetospheric FACs traversing the 3.7-R_E shell are mapped onto the polar cap via the static dipole field. These FACs are used as input for the ionospheric potential equation

$$\nabla \cdot \underline{\underline{\Sigma}} \cdot \nabla \Phi = -j_{||} \sin I$$

which is solved on the surface of a sphere with radius 1 R_E and centered on Earth. Here, Φ denotes the ionospheric potential, $\underline{\underline{\Sigma}}$ is the tensor for ionospheric conductance, $j_{||}$ is the mapped FAC with the downward current as positive and corrections for flux tube convergence, and I is the inclination of the dipole field at the ionosphere. The boundary condition $\Phi = 0$ is applied at the equator. For the ionospheric Hall and Pedersen conductances Σ_H and Σ_P [*Kamide and Matsushita,* 1979], three ionization sources are taken into account. First, the model of *Moen and Brekke* [1993] is used for the solar EUV ionization. Second, the mean energy and energy flux of precipitating electrons associated with the upward FACs is computed from the relationship given by *Lyons et al.* [1979]. Third, the diffuse electron precipitation is modeled with the assumption of strong pitch angle scattering of electrons at 3.7 R_E. The empirical relations for electron precipitation as given by *Hardy et al.* [1987] are then used to compute the conductances. With these ionospheric conductances and the mapped FACs the potential equation is solved. Then the ionospheric potential is mapped to the 3.7-R_E shell where it is used as a boundary condition for the magnetospheric flow, $\mathbf{v} = (-\nabla\Phi) \times \mathbf{B} / B^2$.

In order to initiate the simulation model the magnetic field is assumed to be that from the superposition of Earth's dipole over a mirror dipole such that $B_x = 0$ at $X = 16$ R_E. Sunward of the symmetry plane at 16 R_E the field is replaced by the initial interplanetary field. This procedure ensures a divergence-free transition from the interplanetary field to Earth's dipolar field. The simulation box is initially filled with tenuous (0.1 cm^{-3}), cold (5000 K) plasma with no bulk velocity. The solar wind flow (v = 500 km/s, ρ = 13 amu/cm^3, T = 300,000 K, and B_z = -4.3 nT) is switched on at the sunward boundary at $t = 0$, and the system is allowed to evolve under these conditions for 90 min, or approximately the time required to pass once through the simulation box. Comparison of runs with different initial conditions shows that the specific initial conditions have only a minimal effect on the structure of the magnetosphere after time periods with this scale. That is, the southward IMF conditions allow a neutral line (at about $X = -25$ R_E) and fast tailward flows to evolve, which clear the magnetotail of any structures that are present due to the initial conditions. After this initial phase the values for the IMF, By and Bz, as observed with IMP 8 are used with 1-min resolution in order to investigate the dynamical behavior of the model magnetotail and its relationship to the observations of cold ion beams in the distant magnetotail with the Geotail spacecraft. Because the Rankine-Hugoniot relations specify that the normal component of **B** does not change across a discontinuity, Bx must be constant for our simulation geometry and has been taken here as $Bx = 0$.

4. Comparison of Observations With the Model Results

A steady solar wind with density of 13 amu/cm^3 and speed of 500 km/s is assumed in the simulation of the magnetotail with the MHD-Ionosphere model that was described in the preceding section. For these computations the flow velocity of the solar wind is along the -X direction. For the period of most intensive analysis here, 0526 to 0545 UT, this solar wind flow direction is well approximated within the accuracies anticipated for the modeled parameters. The aberration of the solar wind by Earth's motion around the Sun is subsequently included in order to locate

the spacecraft in the modeled magnetotail. At the position of the Geotail spacecraft, $X = 81\ R_E$, this aberration is 4.9 R_E in the $+Y$ direction. The ion densities and temperatures and the components of the bulk flow velocities that are computed for the Geotail position are shown in Figure 3. The observed values of these parameters are also displayed in this figure in the same format in which these data are shown in Figure 1. The computed densities in the upper panel do not exhibit the large decreases in density for the intervals between the appearances of the cold ion stream, i.e., for the magnetotail lobe. This effect is probably due to the fact that the density gradients at the edges of the streams are considerably steeper than can be accounted for by the spatial resolution of the computer model. This appears to be supported by the fact that the computed densities fall to lower values when the interval for the presence of the lobe is longer, i.e., the intervals 0330–0410 UT and 0550–0630 UT, and thus presumably with deeper penetration into the lobe. The computed and observed densities within the cold ion stream are in good agreement.

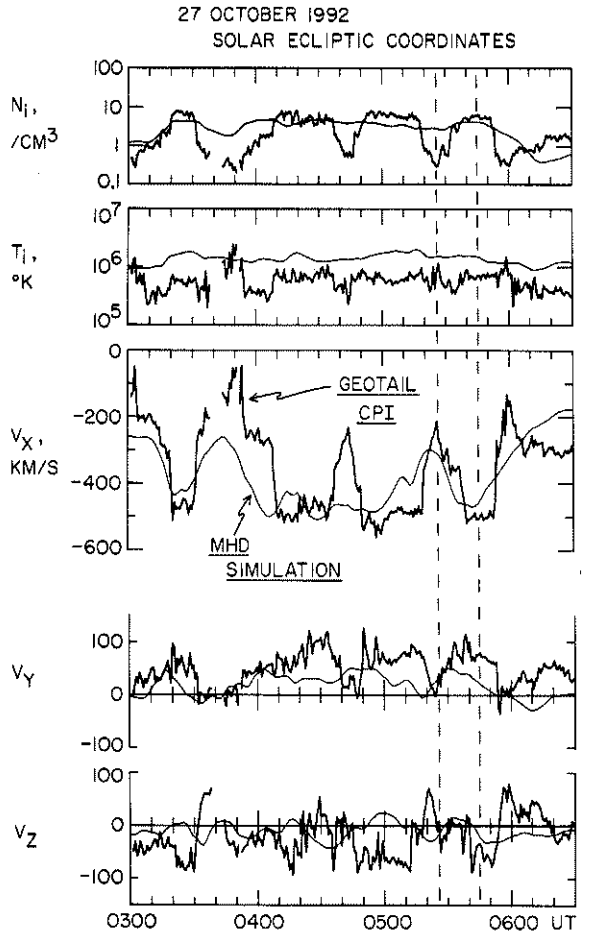

Figure 3. Comparison of the ion plasma parameters in the distant magnetotail as observed with the Geotail spacecraft (thick lines) with the computed plasma parameters as gained with a global MHD–Ionosphere model (thin lines). The IMF and solar wind ion parameters as measured with IMP 8 are used as input to the model.

The computed ion temperatures as shown in the second panel of Figure 3 are about a factor of 2 larger than those observed at the Geotail position. Both computed and observed values do not display large fluctuations. Comparison of the calculated tailward components of bulk flows shown in the third panel shows reasonable qualitative and quantitative agreement with the measured values in consideration of the complexity of the phenomena. Further, the computed and observed bulk flows exhibit a fluctuating, but persistent, duskward motion ($+V_y$). The bottom panel summarizes the computed and observed Z components of the bulk flows. Because the elevation angle for the solar wind flow for input to the model is assumed to be constant and parallel to the ecliptic plane, some of the disparities for this latter component may be due to fluctuations of the solar wind direction. Because only the one cycle of beam appearance during 0520–0610 UT is well covered by IMP 8 plasma measurements (see Figure 1), we will concentrate on this interval in our later discussion. In particular, the deflection of the cold ion stream in the –Z direction for the observations and the model at about 0546 UT is examined in detail. This deflection is not due to a southerly deflection of the solar wind ion beam.

The computed magnetic fields at the position of the Geotail spacecraft are shown in Figure 4. For Bx the greatest discrepancies occur during the interval of 0410–0445 UT when the spacecraft is located in and

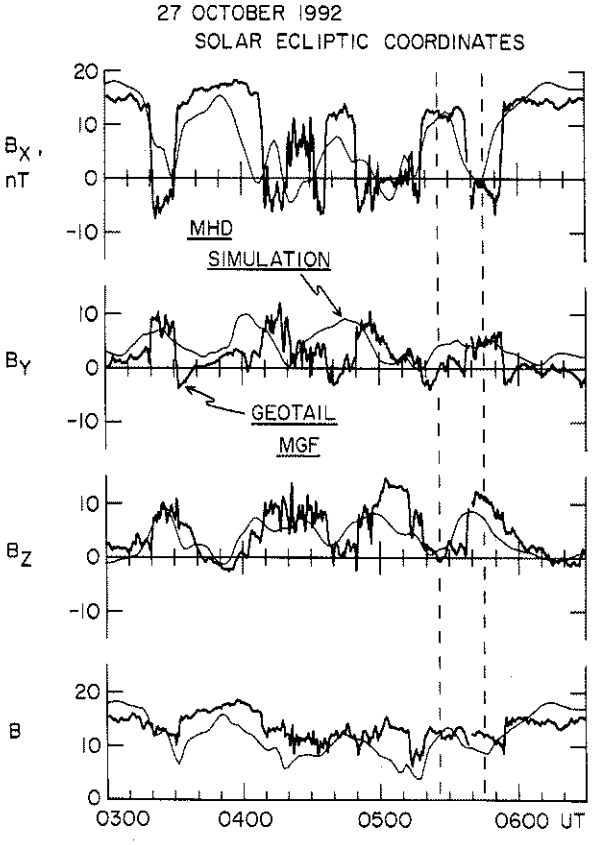

Figure 4. Continuation of Figure 3 for observed and computed magnetic fields at the Geotail position.

near the boundary between the magnetotail lobe and cold ion stream. For such a situation the model results can be reasonably expected to differ. This difference can also be attributed in part to the fact that the X component of the IMF is assumed to be zero for the simulation. The Y components of the modeled fields display a profile that is similar to that for the observed values. However, there is a notable phase lead in the computed values. This discrepancy may arise from faster Alfvén speeds for the modeled fields and densities. This phase lead is not as great for the Z component of the magnetic fields shown in the third panel in Figure 4. Overall the agreement between the computed and observed magnetic fields is sufficiently good to give confidence that the gross global configuration of the magnetotail that the model provides is valid.

The MHD–Ionosphere model provides insight into the global geometry of the magnetotail. As anticipated, the topology of the magnetic field is complex. The state of the magnetotail is discussed in detail for two times, 0526 UT during a period when the Geotail spacecraft is in the lobe and for which the Y component of the IMF is strongly positive (duskward) and 0545 UT. It is during this latter interval that the cold ion stream is present at the spacecraft position and the IMF has rotated northward. These two times are indicated by the two vertical dashed lines in Figures 1, 2, 3, and 4. A sampling of the configurations of the magnetic field lines that pass near the position of the Geotail spacecraft is given in Plate 2. As shown in the left-hand side of Plate 2, the spacecraft is located on open field lines that are connected to Earth's northern polar cap at 0526 UT. For the period with small By during 0545 UT the geometry of the magnetotail has changed such that the Geotail spacecraft is positioned at the boundary between such open field lines and a region of field lines unconnected with those of the terrestrial magnetic field. Examples of closed field lines are also shown in the two diagrams of Plate 2.

Because the magnetic field topologies shown in Plate 2 are complex and the geometries are difficult to visualize, cross-sectional summaries of the magnetic field topologies have been developed and are shown in Plate 3. These cross sections in the Y–Z plane are taken at the position of the Geotail spacecraft at $X = -81\ R_E$. The magnetic field topologies are identified in the plate legend. The spacecraft position is indicated by the circled white point with black center. Note that the spatial geometry of the regions with closed field lines is quite complex. The positive X axis is directed away from the viewer. At 0526 UT the magnetotail geometry is such that the spacecraft is located in a region of closed and open field lines. At 0545 UT the cold ion stream has appeared at the spacecraft position which is located at the boundary between open and unconnected field lines.

Cross-sectional views of the ion densities are shown in Plate 4 in the same format as that used for Plate 3. The downstream distance is again $X = -81\ R_E$. A small increase in these densities is predicted by the model with the appearance of the cold ion stream at 0545 UT relative to the densities in the magnetotail lobe at the spacecraft position at 0526 UT. As noted earlier, the observed density increases are considerably greater, as can be easily seen in Figure 3. That is, the observed spatial gradients are steeper. However, sufficiently low densities to match the measured densities are found somewhat deeper into the magnetotail lobes in Plate 4. Thus this quantitative discrepancy in the density gradient is expected to be reduced with increasing resolution in the models as the computer capabilities improve.

The Y component of the current densities in the modeled magnetotail is shown in the cross-sectional view in Plate 5. At 0526 UT the Geotail spacecraft is located in a region of relatively weak current density in the northern lobe. For the strongly positive values of IMF B_y the magnetotail is rotated and deformed in such a manner as to position the magnetotail lobe at the Geotail spacecraft. The rotation is also seen in the distribution of cross-tail currents in the magnetotail current sheet that is located nearer the Y axis. During the northward IMF at 0546 UT the geometry of the magnetotail is such that the magnetopause currents are found near the spacecraft position.

Plate 6 displays cross-sectional plots for the Z component of ion bulk flows, again at 0526 UT and 0545 UT. The magnetosheath flows are clearly seen at the tops and bottoms of these plots. The flows inside the magnetopause are quite complex. The magnetopause positions are easily identifiable in the cross sections of the previous Plate 5. We have noted previously a subtle aspect of the observed dynamical behavior of the magnetotail, i.e., the southward deflection of the ion bulk flow in the cold ion stream that appeared at the Geotail position at 0545 UT (see Figure 2). Examination of the Z components of ion bulk flows for the modeled magnetotail in Plate 6 indeed finds the same southerly deflection of bulk flows relative to those computed for 0526 UT. This positive correlation of measured and computed flows provides substantial confidence in the robustness of the model magnetotail.

Another prominent feature of the observed plasma flows is the duskward (+Y) deflection for both the magnetotail lobe plasmas and those of the cold ion streams (see Figure 1). The Y component for the solar wind flow at IMP 8 is considerably smaller. The MHD model also predicts the positive deflection for the lobe and the cold ion stream. Cross sections for the Y components of bulk flow are shown in Plate 7. These cross-sectional views exhibit the considerable complexity of the motions of plasmas in the magnetotail and their great variability in response to the direction of the IMF.

5. Summary and Discussion

We have presented our findings from an exploratory comparison of a series of observations of plasmas and magnetic fields in Earth's distant magnetotail with the simulation results from a global MHD model

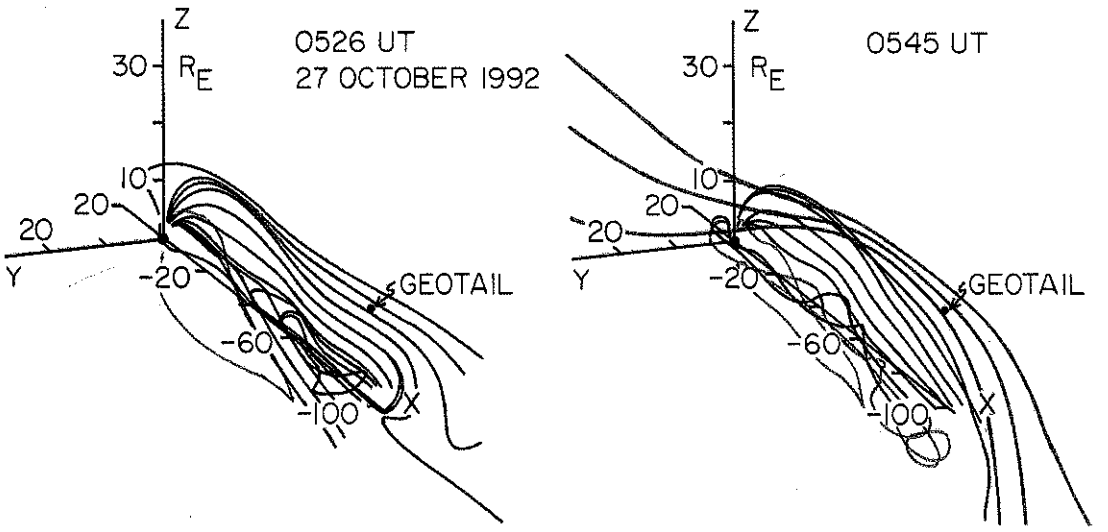

Plate 2. Diagrams showing the three-dimensional topologies of the magnetic field lines in the vicinity of the Geotail spacecraft as computed with the MHD-Ionosphere model at 0526 UT when the spacecraft was located in the northern lobe (left-hand side) and at 0545 UT when the cold, dense ion stream appeared at the spacecraft (right-hand side). Closed magnetic field lines (both feet on Earth, green), open field lines (one foot on Earth, blue) and unconnected (interplanetary, red) are shown.

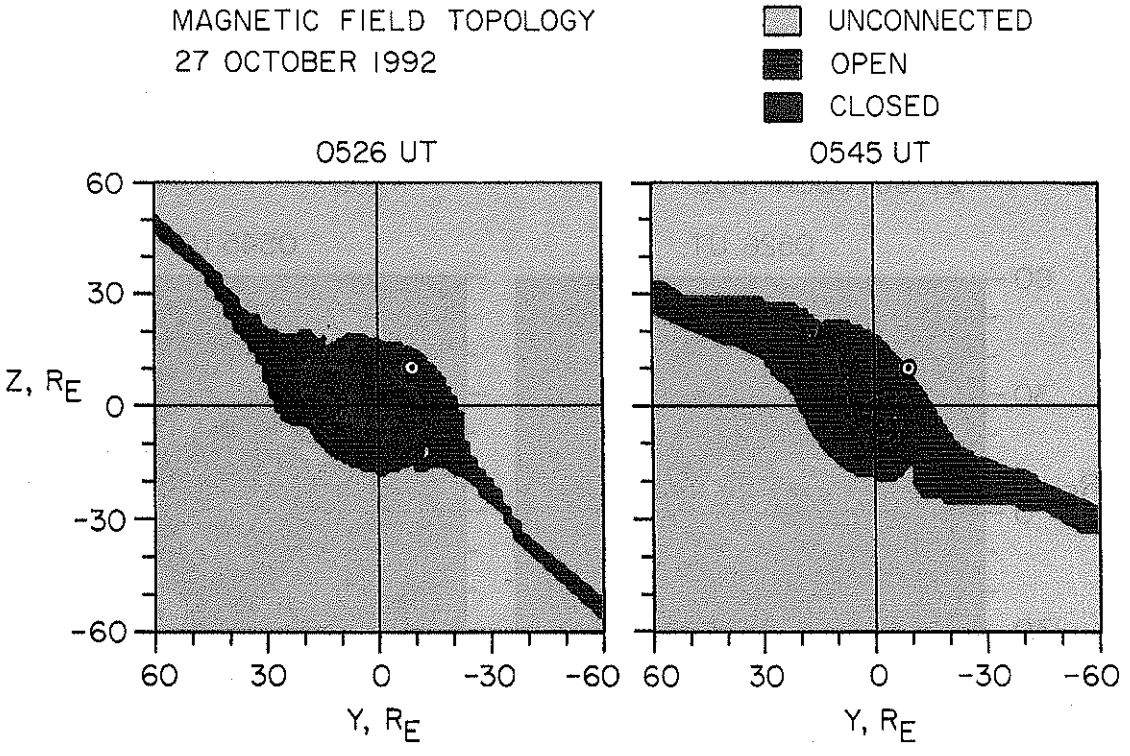

Plate 3. Cross-sectional views of the topology of the magnetic field lines crossing the Y-Z plane at $X = -81\ R_E$ (Earth-centered solar-ecliptic coordinates). An aberration of $4.9\ R_E$ along the $+Y$ axis has been included to account for the orbital motion of Earth. These maps have been computed with the MHD-Ionosphere model for 0526 UT (left) and 0545 (right) when the Geotail spacecraft (white dot) was within the magnetotail lobe and the dense, cold ion stream, respectively. These times are indicated by the vertical dashed lines in Figures 1, 2, 3, and 4. Note that at 0545 UT the model places the spacecraft at the boundary between open and unconnected field lines.

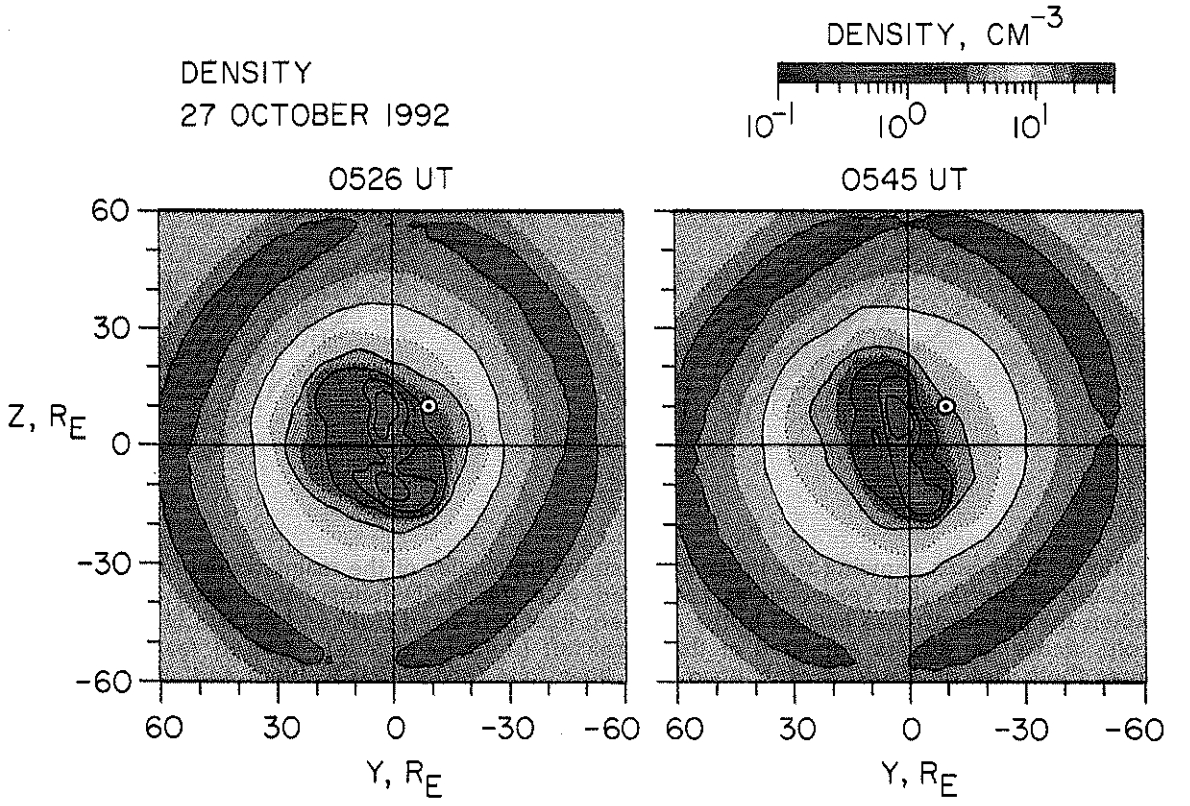

Plate 4. Continuation of Plate 3 for the modeled ion densities.

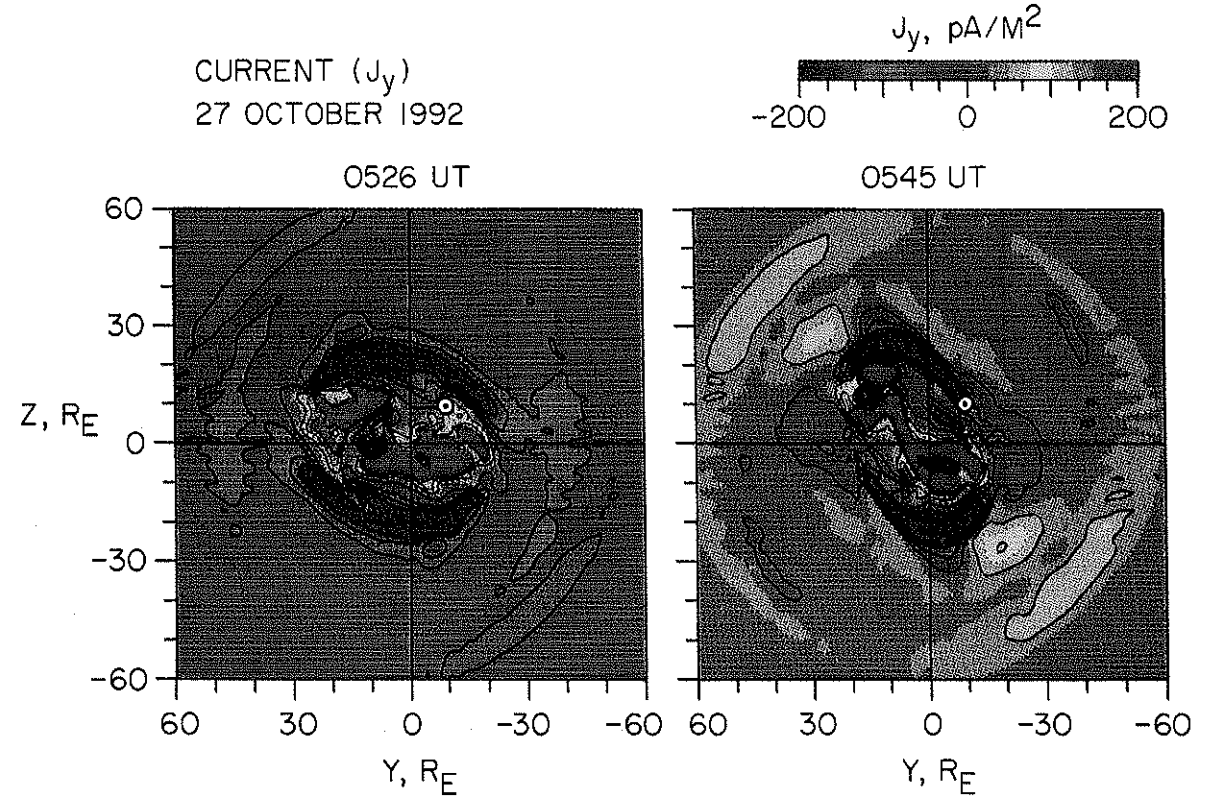

Plate 5. Continuation of Plate 3 for the Y component of the modeled current densities. Current densities at the Geotail position in the lobe at 0526 UT are relatively low, as expected, and the model places this spacecraft near the magnetopause current layer when the dense, cold ion stream is detected at 0545 UT.

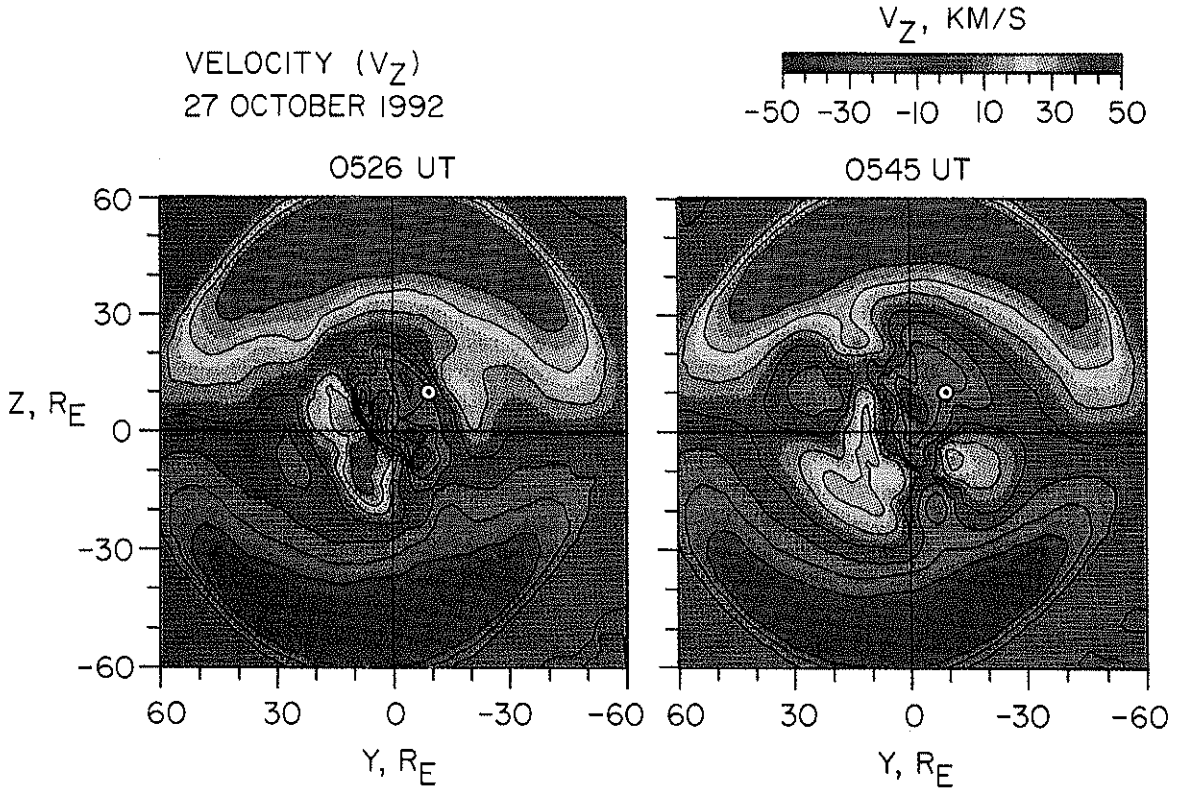

Plate 6. Continuation of Plate 3 for the Z component of the ion bulk flow velocity. The model accounts for a subtle feature of the observed plasmas, i.e., the southward deflection of the cold, dense ion stream at 0545 UT. Also see Figures 1 and 2.

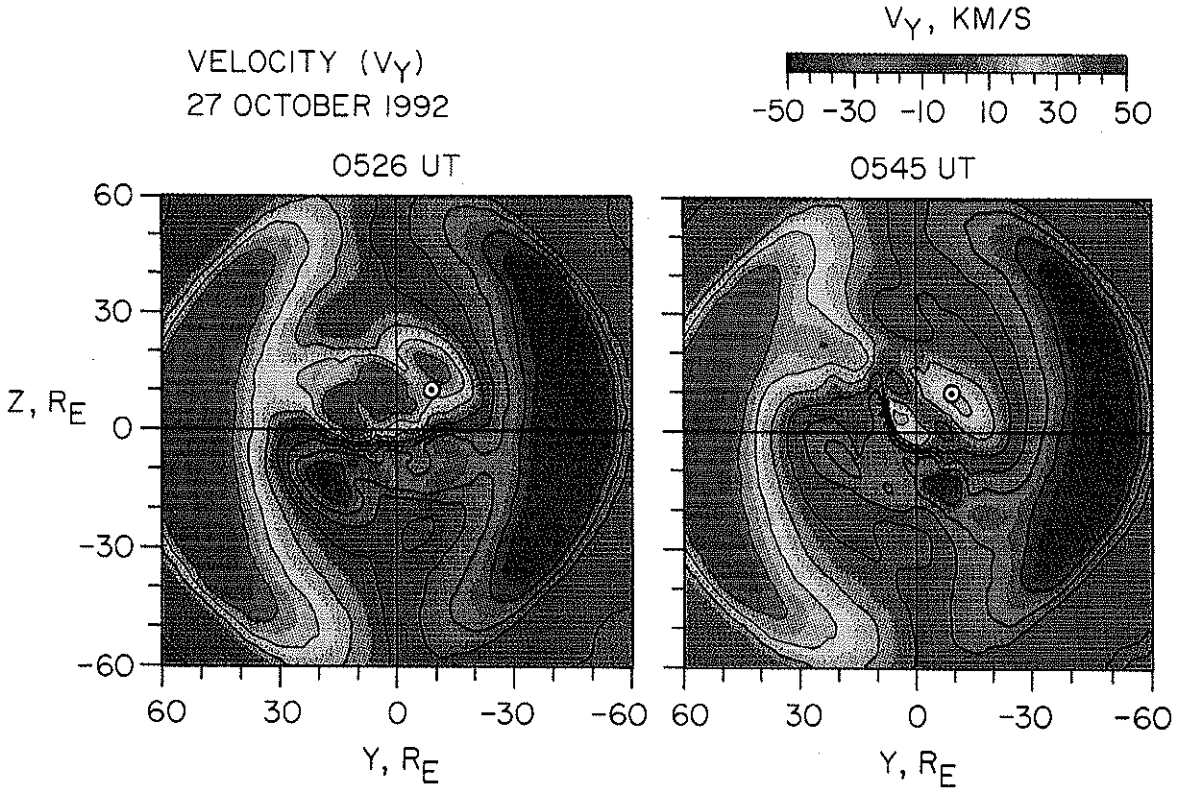

Plate 7. Continuation of Plate 3 for the Y component of the ion bulk flow velocity. Note that the model predicts the duskward deflection of plasmas for both the lobe plasmas and the cold streams which is observed with the Geotail spacecraft.

of the interaction of the solar wind with the magnetosphere. To our knowledge there are no previously reported efforts to directly compare model results with a time series of observed plasma parameters. These observations were obtained with the Geotail spacecraft at a downstream distance of about 81 R_E in the vicinity of the dawnside magnetopause. This particular series of observations was chosen because a dense, cold stream of ions appeared intermittently at the spacecraft position. When this ion beam was not present, the spacecraft was located in the northern magnetotail lobe. This situation indicated that the magnetotail was in an active dynamical state in response to fluctuations in one or more parameters in the interplanetary medium. In addition, simultaneous observations of the solar wind ions and the IMF were available from the IMP 8 spacecraft. The overall observational situation was judged to provide an excellent test of the ability of a MHD model to account for the large-scale structure and dynamics of the magnetotail.

The solar wind ion beam was observed by IMP 8 to be steady with a density of about 13 protons/cm^3 and speed of 500 km/s. The IMF was characterized by a substantial rotation between northward and duskward directions. When the Y component was strongly positive (duskward), the magnetotail was reconfigured such that the Geotail spacecraft was located in the northern magnetotail lobe. The other periods with generally northward IMF found this spacecraft within the dense, cold ion stream. This cold ion stream exhibited densities, temperatures, and bulk speeds that were similar to those expected for the far downstream magnetosheath, i.e., similar to those for the interplanetary medium. However, there were several features of the cold stream that indicated that this plasma was influenced by the nearby presence of the magnetopause. These features were the deflection of the ion beam in the $-Z$ and $+Y$ directions and positive values of the Y component of the magnetic field when this IMF component was negative or small.

This layer of magnetosheathlike plasmas can be distinguished from the magnetosheath only with comprehensive and precise determinations of the three-dimensional velocity distributions of ions. These magnetosheathlike plasmas, otherwise referred to herein as cold ion streams, are positioned just outside and contiguous to the classical magnetopause as determined by the rapid transition from well-ordered, approximately Sun-aligned magnetic fields of the magnetotail lobe to fluctuating, lesser fields of the magnetosheath. Plasmas that are probably associated with the plasma mantle are to be found on lobe field lines. Their densities and bulk speeds are lesser than those for the cold ion streams. Thus the structure of the downstream magnetopause region and its dynamics are considerably more complex than was previously thought. It is important to also note that *Williams et al.* [1994] have observed fluxes of energetic ions that spatially straddle the classical magnetic signature of the magnetopause for the series of observations reported here and are interpreted in terms of acceleration and injection along the downstream magnetopause.

The global MHD-Ionosphere model [*Raeder et al.*, 1995; *Berchem et al.*, 1995] was investigated in order to determine its ability to account for the topology and dynamical behavior of the magnetotail during the above series of observations. The driving inputs for the model were the above values for a steady solar wind ion beam and the observed values for the fluctuating Y and Z components of the IMF with 1-min time resolution. An aberration of 3.4° in the magnetotail accounted for the Earth's orbital motion. The modeled results were directly compared with the Geotail observations during a period of several hours. The model correctly predicted the intervals for the appearance of the cold ion streams and of the northern magnetotail lobe at the Geotail position. Examination of the temporal profiles of the observed and modeled parameters found good qualitative agreement. These parameters were the ion density, temperature, and bulk velocity and the components of the magnetic field. The major discrepancies were the high lobe densities, greater ion temperatures, and the phase lead in the Y component of the magnetic field relative to the observed values (see Figures 3 and 4). The high lobe densities are probably due to the inability of the present spatial resolution of the model to account for the steep spatial gradient in the vicinity of the magnetopause. The phase lead of the Y component of the magnetic field is probably related to differences in the Alfvén speeds in the model relative to those for the actual magnetosphere.

Cross sections of the modeled plasma parameters in the Y-Z plane through the position of the Geotail spacecraft were valuable in assessing their relationship with the single-point in situ observations. The plasma parameters presented in this manner were the density, the Y component of the current density, and the Y and Z components of the ion bulk flow. In addition, cross sections of the field topology were also presented, i.e., whether the magnetic field line was closed, open, or unconnected at its intersection with the Y-Z plane (see Plate 3). The cross sections for all of the above features are given for two times, 0526 UT and 0545 UT, which correspond to the presence of the lobe and of the cold ion stream, respectively, at the Geotail spacecraft. The ability of the model to predict the sequence of appearances of these regions at the spacecraft lends considerable credibility to the gross global features portrayed in these cross sections. The clockwise twisting of the magnetotail as viewed toward Earth in response to the torque exerted about its central (X) axis by the Y component of the IMF as previously suggested by *Cowley* [1981] for weak values of the Z component is clearly evident in the current densities shown in Plate 5. However, the details of their distribution are vastly more complex than the early sketches.

One of the more subtle features of the dense, cold ion stream is its southward deflection of flow, in the range of a few tens of kilometers per second. The

cross-sectional view of this Z component of ion bulk flow displayed in Plate 6 shows that the global MHD model is able to account for this southward deflection.

The character of the perturbations of the plasma flow and magnetic fields in the region just outside the classical magnetopause, together with the complex geometry of the magnetopause as derived from the MHD model, provides considerable evidence that the magnetosheath plasmas are accommodating the structure of the magnetopause. Thus we refer to a "magnetopause accommodation region."

The overall agreement of the modeled results and the observations with the Geotail spacecraft for a single position in the region of the dawnside magnetopause provides ample motivation to improve and further verify the robustness of the model. This work will be extended with observations in other regions of the magnetotail and under other conditions for the solar wind ions and the IMF. It is clear that this MHD–Ionosphere model can give significant insight into the global topology of such magnetotail regions as the lobe, the magnetopause, and the downstream plasma mantle and can provide their dynamical responses due to temporal fluctuations of plasmas and magnetic fields in the interplanetary medium.

Regardless of these remarkable successes for the MHD model, it has been previously shown that the concept of resistivity for the magnetotail current sheet will not be understood on fundamental physical grounds from such modeling. The motions of ions in the plasma sheet have been shown to be nonadiabatic via the determination of their complex three-dimensional velocity distributions [*Frank et al.*, 1994a]. It is possible that the electron motion in the plasma sheet is also nonadiabatic to a lesser extent. In order to understand the topology and dynamics of the plasma sheet it is necessary to model this critical magnetotail region with large-scale kinetic simulations based upon such previous work as that of *Speiser* [1965], *Lyons and Speiser* [1982], and *Ashour-Abdalla et al.* [1993] and with nonlinear dynamical formulations such as those offered by *Chen and Palmadesso* [1986] and *Chen* [1992]. The path for providing a magnetotail model based upon fundamental principles is becoming increasing well defined in that the MHD modeling will provide the basic magnetic field topology and plasma distributions in the magnetotail but not within the plasma sheet and its boundary layer. This latter region is to be understood with numerical simulations of the collective nonadiabatic motions of charged particles in the cross-tail electric fields and weak magnetic fields in the magnetotail current sheet. The greatest hurdle in constructing this comprehensive global model will probably arise from the self-consistent integration of the MHD and kinetic models.

Acknowledgments. The IMP 8 plasma measurements in the solar wind were kindly supplied by A. J. Lazarus and K. Paularena of the Massachusetts Institute of Technology. This research was supported in part at The University of Iowa under NASA grant NAG5-2371 and at the University of California at Los Angeles under NASA ISTP grant NAG5-1100 and University of Iowa subcontract V26073. The model computations were performed on the Paragon at the San Diego Supercomputer Center.

The Editor thanks J. B. Cladis and another referee for their assistance in evaluating this paper.

References

Ashour-Abdalla, M., J. Berchem, J. Büchner, and L. Zelenyi, Shaping of the magnetotail from the mantle: Global and local structuring, *J. Geophys. Res.*, *98*, 5651–5676, 1993.

Bame, S. J., R. C. Anderson, J. R. Asbridge, D. N. Baker, W. C. Feldman, J. T. Gosling, E. W. Hones Jr., D. J. McComas, and R. D. Zwickl, Plasma regimes in the deep geomagnetic tail: ISEE 3, *Geophys. Res. Lett.*, *10*, 912–915, 1983.

Bellomo, A., and A. Mavretic, MIT plasma experiment on IMP H and J Earth orbited satellites, *Intern. Rep. CSR TR-78-2*, Cent. for Space Res., Mass. Inst. of Technol., Cambridge, 1978.

Berchem, J., J. Raeder, and M. Ashour-Abdalla, Reconnection at the magnetospheric boundary: Results from global magnetohydrodynamic simulations, in *Geophysical Monograph Series*, edited by B. U. O. Sonnerup, P. Song, and M. Thomsen, in press, 1995.

Brecht, S. H., J. G. Lyon, J. A. Fedder, and K. Hain, A time dependent three-dimensional simulation of the Earth's magnetosphere: Reconnection events, *J. Geophys. Res.*, *87*, 6098–6108, 1982.

Chen, J., Nonlinear dynamics of charged particles in the magnetotail, *J. Geophys. Res.*, *97*, 15,011–15,050, 1992.

Chen, J., and P. J. Palmadesso, Chaos and nonlinear dynamics of single-particle orbits in a magnetotail-like magnetic field, *J. Geophys. Res.*, *91*, 1499–1508, 1986.

Cowley, S. W. H., Magnetospheric asymmetries associated with the Y-component of the IMF, *Planet. Space Sci.*, *29*, 79–96, 1981.

Evans, C. R., and J. F. Hawley, Simulation of magnetohydrodynamic flows: A constrained transport method, *Astrophys. J.*, *332*, 659–677, 1988.

Fairfield, D. H., Average and unusual locations of the Earth's magnetopause and bow shock, *J. Geophys. Res.*, *76*, 6700–6716, 1971.

Fedder, J. A., and J. G. Lyon, The solar wind–magnetosphere–ionosphere current–voltage relationship, *Geophys. Res. Lett.*, *14*, 880–883, 1987.

Fedder, J. A., C. M. Mobarry, and J. G. Lyon, Reconnection voltage as a function of IMF clock angle, *Geophys. Res. Lett.*, *18*, 1047–1050, 1991.

Frank, L. A., and W. R. Paterson, Survey of electron and ion bulk flows in the distant magnetotail with the Geotail spacecraft, *Geophys. Res. Lett.*, *21*, 2963–2966, 1994.

Frank, L. A., W. R. Paterson, and M. G. Kivelson, Galileo observations of the motions of ion and electron plasmas in the magnetotail, *Geophys. Res. Lett.*, *20*, 1771–1774, 1993.

Frank, L. A., W. R. Paterson, and M. G. Kivelson, Observations of nonadiabatic acceleration of ions in Earth's magnetotail, *J. Geophys. Res.*, *99*, 14,877–14,890, 1994a.

Frank, L. A., K. L. Ackerson, W. R. Paterson, J. A. Lee, M. R. English, and G. L. Pickett, The Comprehensive Plasma Instrumentation (CPI) for the GEOTAIL spacecraft, *J. Geomagn. Geoelectr.*, *46*, 23–37, 1994b.

Frank, L. A., W. R. Paterson, K. L. Ackerson, S. Kokubun, T. Yamamoto, D. H. Fairfield, and R. P. Lepping, Observations of plasmas associated with the magnetic signature of a plasmoid in the distant magnetotail, *Geophys. Res. Lett.*, *21*, 2967–2970, 1994c.

Hardy, D. A., M. S. Gussenhoven, R. Raistrick, and W. J. McNeil, Statistical and functional representations of the pattern of auroral energy flux, number flux, and conductivity, *J. Geophys. Res.*, *92*, 12,275–12,294, 1987.

Harten, A., and G. Zwas, Self-adjusting hybrid schemes for shock computations, *J. Comput. Phys.*, *9*, 568–583, 1972.

Hirsch, C., Numerical computation of internal and external flows, in *Computational Methods for Inviscid and Viscous Flows*, vol. 2, 691 pp., John Wiley, New York, 1990.

Howe, H. C., Jr., and J. H. Binsack, Explorer 33 and 35 plasma observations of magnetosheath flow, *J. Geophys. Res.*, *77*, 3334–3344, 1972.

Kamide, T., and S. Matsushita, Simulation studies of ionospheric electric fields and currents in relation to field-aligned currents, 1, Quiet periods, *J. Geophys. Res.*, *84*, 4083–4098, 1979.

Kokubun, S., T. Yamamoto, M. H. Acuña, K. Hayashi, K. Shiokawa, and H. Kawano, The GEOTAIL magnetic field experiment, *J. Geomagn. Geoelectr.*, *46*, 7–21, 1994.

LeBoeuf, J. N., T. Tajima, C. F. Kennel, and J. M. Dawson, Global simulation of the time-dependent magnetosphere, *Geophys. Res. Lett.*, *5*, 609–612, 1978.

LeBoeuf, J. N., T. Tajima, C. F. Kennel, and J. M. Dawson, Global simulations of the three-dimensional magnetosphere, *Geophys. Res. Lett.*, *8*, 257–260, 1981.

Lepping, R. P., A. J. Lazarus, L. J. Moriarity, P. Milligan, R. S. Kennon, R. E. McGuire, and W. H. Mish, IMP-8 solar wind magnetic field and plasma data in support of ULYSSES-Jupiter Encounter: 13–31 January 1992, Intern. Doc., Lab. for Extraterrestrial Phys., Goddard Space Flight Cent./NASA, Greenbelt, Md., 1992.

Lyon, J. G., S. H. Brecht, J. D. Huba, J. A. Fedder, and P. J. Palmadesso, Computer simulation of a geomagnetic substorm, *Phys. Rev. Lett.*, *46*, 1038–1041, 1981.

Lyons, L. R., and T. W. Speiser, Evidence for current sheet acceleration in the geomagnetic tail, *J. Geophys. Res.*, *87*, 2276–2286, 1982.

Lyons, L. R., D. S. Evans, and R. Lundin, An observed relation between magnetic field aligned electric fields and downward electron energy fluxes in the vicinity of auroral forms, *J. Geophys. Res.*, *84*, 457–461, 1979.

Moen, J., and A. Brekke, The solar flux influence on quiet time conductances in the auroral ionosphere, *Geophys. Res. Lett.*, *20*, 971–974, 1993.

Ogino, T., A three-dimensional MHD simulation of the interaction of the solar wind with the Earth's magnetosphere: The generation of field-aligned currents, *J. Geophys. Res.*, *91*, 6791–6806, 1986.

Ogino, T., R. J. Walker, and M. Ashour-Abdalla, A global magnetohydrodynamic simulation of the magnetosheath and the magnetosphere when the interplanetary magnetic field is northward, *IEEE Trans. Plasma Sci.*, *20*, 817–828, 1992.

Ogino, T., R. J. Walker, and M. Ashour-Abdalla, A global magnetohydrodynamic simulation of the response of the magnetosphere to a northward turning of the interplanetary magnetic field, *J. Geophys. Res.*, *99*, 11,027–11,042, 1994.

Paterson, W. R., and L. A. Frank, Survey of plasma parameters in Earth's distant magnetotail with the Geotail spacecraft, *Geophys. Res. Lett.*, *21*, 2971–2974, 1994.

Petrinec, S. P., P. Song, and C. T. Russell, Solar cycle variations in the size and shape of the magnetopause, *J. Geophys. Res.*, *96*, 7893–7896, 1991.

Raeder, J., Global MHD simulations of the dynamics of the magnetosphere: Weak and strong solar wind forcing, in *Proceedings of the Second International Conference on Substorms*, eds. J. R. Kan, J. D. Craven and S.-I. Akasofu, pp. 561–568, Univ. of Alaska Press, Fairbanks, 1994.

Raeder, J., R. J. Walker, and M. Ashour-Abdalla, The structure of the distant geomagnetic tail during long periods of northward IMF, *Geophys. Res. Lett.*, *22*, 349–352, 1995.

Russanov, V. V., Calculation of interaction of non-steady shock waves with obstacles, Translation 1027, *J. Comput. Math. Phys.*, no. 2, 1962.

Sato, T., and T. Hayashi, Externally driven magnetic reconnection and a powerful magnetic energy converter, *Phys. Fluids*, *22*, 1189–1202, 1979.

Slavin, J. A., and R. E. Holzer, Solar wind flow about the terrestrial planets, 1, Modeling bow shock position and shape, *J. Geophys. Res.*, *86*, 11,401–11,418, 1981.

Slavin, J. A., E. J. Smith, D. G. Sibeck, D. N. Baker, R. D. Zwickl, and S.-I. Akasofu, An ISEE 3 study of average and substorm conditions in the distant magnetotail, *J. Geophys. Res.*, *90*, 10,875–10,895, 1985.

Speiser, T. W., Particle trajectories in model current sheets, 1, Analytical solutions, *J. Geophys. Res.*, *70*, 4219–4226, 1965.

Ugai, M., Temporal evolution and propagation of a plasmoid associated with asymmetric fast reconnection, *J. Geophys. Res.*, *90*, 9576–9582, 1985.

Usadi, A., A. Kageyama, K. Watanabe, and T. Sato, A global simulation of the magnetosphere with a long tail: Southward and northward interplanetary magnetic field, *J. Geophys. Res.*, *98*, 7503–7517, 1993.

Walker, R. J., T. Ogino, J. Raeder, and M. Ashour-Abdalla, A global magnetohydrodynamic simulation of the magnetosphere when the interplanetary magnetic field is southward: The onset of magnetotail reconnection, *J. Geophys. Res.*, *98*, 17,235–17,249, 1993.

Watanabe, K., and T. Sato, Global simulation of the solar wind-magnetosphere interaction: The importance of its numerical validity, *J. Geophys. Res.*, *95*, 75–88, 1990.

Williams, D. J. et al., Magnetopause encounters in the magnetotail at distances of ~80 R_E, *Geophys. Res. Lett.*, *21*, 3007–3010, 1994.

Wu, C. C., R. J. Walker, and J. M. Dawson, A three-dimensional MHD model of the Earth's magnetosphere, *Geophys. Res. Lett.*, *8*, 523–526, 1981.

K. L. Ackerson, L. A. Frank, and W. R. Paterson, Department of Physics and Astronomy, University of Iowa, Iowa City, IA 52242. (e-mail: ackerson@iowasp.physics.uiowa.edu; frank@iowasp physics.uiowa.edu; paterson@iowasp.physics.uiowa.edu)

M. Ashour-Abdalla, J. Berchem, and J. Raeder, Institute of Geophysics and Planetary Physics, University of California at Los Angeles, Los Angeles, CA 90024. (e-mail: mabdalla@igpp.ucla.edu; jberchem@igpp.ucla.edu; jraeder @igpp.ucla.edu)

F. V. Coroniti, Department of Physics and Astronomy, University of California at Los Angeles, Los Angeles, CA 90024. (e-mail: chairman@physics.ucla.edu)

D. H. Fairfield and R. P. Lepping, NASA/Goddard Space Flight Center, Greenbelt, MD 20771. (e-mail: u2dhf@lepdhf.gsfc.nasa.gov; rpl@leprpl.gsfc.nasa.gov)

S. Kokubun, Solar-Terrestrial Environment Laboratory, Nagoya University, 3–13 Honohara, Toyokawa, Aichi 442, Japan. (e-mail: kokubun@stelab.nagoya-u.ac.jp)

T. Yamamoto, Institute of Space and Astronautical Science, Sagamihara, Kanagawa 229, Japan. (e-mail: yamamoto@fujitubo.gtl.isas.ac.jp)

(Received September 19, 1994; revised December 6, 1994; accepted February 10, 1995.)